Chinese Journal of Catalysis 38 (2017) 928–938

available at www.sciencedirect.com

ScienceDirect

journal homepage: www.elsevier.com/locate/chnjc

Article

One-step synthesis of pyruvic acid from glycerol oxidation over Pb promoted Pt/activated carbon catalysts

Chen Zhang [a,c], Tao Wang [a,#], Yunjie Ding [a,b,*]

[a] *Dalian National Laboratory for Clean Energy, Dalian Institute of Chemical Physics, Chinese Academy of Sciences, Dalian 116023, Liaoning, China*
[b] *State Key Laboratory of Catalysis, Dalian Institute of Chemical Physics, Chinese Academy of Sciences, Dalian 116023, Liaoning, China*
[c] *University of Chinese Academy of Sciences, Beijing 100049, China*

ARTICLE INFO

Article history:
Received 9 March 2017
Accepted 10 April 2017
Published 5 May 2017

Keywords:
Glycerol oxidation
Pyruvic acid
Lead promoter
Platinum
Activated carbon

ABSTRACT

One-step production of pyruvic acid through selective oxidation of glycerol was investigated using lead promoted platinum/activated carbon (Pb-Pt/AC) catalysts under mild conditions. The results of N_2 physisorption, X-ray diffraction, X-ray photoelectron spectroscopy, and high-resolution transmission electron microscopy revealed that the alloy phases of PtPb and Pt_xPb were favorable for pyruvic acid production from glycerol oxidation, whereas the $Pb_3(CO_3)_2(OH)_2$ and surface Pb^0 species inhibited the glycerol conversion. The loading of Pb and the catalyst preparation method (including impregnation and deposition precipitation) affected the formation of different metal species. Pyruvic acid was obtained at a yield of 18.4% on a 5.0 wt% Pb-5.0 wt% Pt/AC catalyst prepared by co-deposition precipitation method and 500 °C argon treatment.

1. Introduction

The challenges of sustainable development, such as increasing energy consumption, expanding commodity demands, and environmental concerns, are calling for the efficient utilization of renewable resources. As an easily available byproduct of biodiesel production, glycerol has drawn increased attention because of its abundant functional groups [1–3]. Various value-added derivatives from glycerol have been obtained through different reactions, including selective oxidation [4,5], hydrogenolysis [6,7], and dehydration [8,9], increasing the feasibility of using glycerol as a bio-building block. Therefore, to explore new pathways of glycerol conversions and enhance the competitiveness of the biodiesel industry is attractive.

Pyruvic acid (PA) has been widely used as food additives, precursors for drugs and agrochemicals, as well as weight-loss supplements [10,11]. Because of the many promising applications of PA, its commercial market is considerable. PA is produced by fermentation of glucose or dehydrative decarboxylation of tartaric acid [12]. However, the problems of these methods remain challenging because the product separation efficiencies in the biological methods are low, whereas the pyrolysis of tartaric acid consumes a large amount of $KHSO_4$ and energy [13]. Thus, developing renewable alternative pathways to produce PA under mild conditions is highly appealing.

The one-step transformation of glycerol to PA is a potential option with high atom efficiency, which could be an addition to the reported PA production methods, including oxidations of

* Corresponding author. Tel/ Fax: +86-411-84379143; E-mail: dyj@dicp.ac.cn
# Corresponding author. Tel/ Fax: +86-411-84379143; E-mail: wangtao@dicp.ac.cn
This work was supported by the National Natural Science Foundation of China (21176236).
DOI: 10.1016/S1872-2067(17)62835-3 | http://www.sciencedirect.com/science/journal/18722067 | Chin. J. Catal., Vol. 38, No. 5, May 2017

propylene glycol or lactic acid (LA) [14–16]. This one-step pathway is viable in a fermentation method [17], but there are limitations in scaling-up. As for chemical methods, recent progresses on PA production from LA (or lactate) [13,18,19] and LA production from glycerol [20–23] have shed light on this one-step strategy. In liquid-phase LA oxidation to PA, heterogeneous bimetallic catalysts have been frequently adopted [15,18,24]. These catalysts commonly consist of noble metals such as Pt or Pd as active sites, heavy metals such as Pb, Te, and Bi as additives, and carbon as a support [15,18,24]. For glycerol oxidation to LA, we previously reported that a 1.0 wt% Pt/AC catalyst performed well under mild conditions, with almost no PA detected [25]. Hayashi et al. reported that Pb was a key additive for Pd/C catalyst in PA production from LA [15]. Therefore, the introduction of Pb promoter to a Pt/AC catalyst is expected to enhance the product distribution and PA yield during glycerol oxidation.

We report the one-pot production of PA from selective oxidation of glycerol under mild conditions. The Pb loading is optimized for PA selectivity. The Pb-Pt/AC catalysts prepared via different methods are investigated, including impregnation, deposition precipitation, and further calcination under an Ar atmosphere. N_2 physical adsorption, X-ray diffraction (XRD), X-ray photoelectron spectroscopy (XPS), and transmission electron microscopy (TEM) analyses are adopted to uncover the structure-activity relationships of catalysts.

2. Experimental

2.1. Catalyst preparation

A series of Pb-Pt/AC catalysts were prepared by the following methods. The Pt loading was fixed at 5.0 wt% in all Pb-Pt/AC catalysts.

2.1.1. Impregnation and deposition precipitation method (Im-DP)

An amount of $Pb(NO_3)_2$ was dissolved in 4 mL of deionized water and impregnated onto 2.0 g of an activated carbon (AC) support. The sample was dried at 120 °C for 12 h and reduced with H_2 at 400 °C for 4 h. Sequentially, Pt was deposited on the as-prepared Pb/AC sample by a deposition-precipitation method [26]. By changing the loading of lead, a series of *x*Pb-5Pt/AC-Im-DP catalysts were obtained (*x* = 1, 3, 5, and 7 wt%, representing the Pb loading). If the 5Pb-5Pt/AC-Im-DP catalyst was further treated with Ar at 500 °C for 4 h, the obtained catalyst was denoted as 5Pb-5Pt/AC-Im-DP-500Ar. The 5Pt/AC-DP catalyst was prepared by a deposition-precipitation method.

2.1.2. Co-deposition precipitation method (Co-DP)

AC support (2.0 g) was firstly dispersed in 200 mL of deionized water. $Pb(NO_3)_2$ and H_2PtCl_6 were introduced, reduced, and deposited simultaneously on the AC support by a deposition-precipitation method. The catalyst was denoted as 5Pb-5Pt/AC-Co-DP with the loadings of Pt and Pb both at 5.0 wt%. If the catalyst was further treated with Ar at 500 °C for 4 h, it was denoted as 5Pb-5Pt/AC-Co-DP-500Ar.

2.1.3. Co-impregnation method (Co-Im)

An amount of $Pb(NO_3)_2$ and H_2PtCl_6 were added into 4 mL of deionized water and co-impregnated onto 2.0 g of AC support. The sample was dried at 120 °C for 12 h and treated under H_2 or Ar atmosphere at 500 °C for 4 h. The metal loadings were the same as the catalysts in Section 2.1.2. The obtained catalysts were denoted as 5Pb-5Pt/AC-Co-Im-500H_2 and 5Pb-5Pt/AC-Co-Im-500Ar.

2.2. Catalyst characterization

N_2 physical adsorption of the samples was performed on a Quantachrome Autosorb-1 instrument. The samples were degassed at 250 °C for 12 h before testing. The crystalline phases of the catalysts were tested by XRD with Cu $K_{\alpha 1}$ radiation on a PANalytical X'Pert PRO diffractometer at 40 kV and 40 mA. TEM and high-resolution TEM (HR-TEM) were performed on a JEM-2100 electron microscope operating at 200 kV. XPS was performed on a Thermo ESCALAB 250Xi X-ray spectroscopy spectrometer. The monochromatic Al K_α source (1486.6 eV) was operated at 15 kV. The C 1*s* peak at 284.6 eV was adopted for correction of the charging effects.

2.3. Glycerol oxidation reaction

The glycerol oxidation reaction was performed in a 100-mL three-neck flask in an oil bath, with 25.0 g of glycerol solution (10.0 wt%), 1.90 g of $LiOH{\cdot}H_2O$ (purity at 90%) and 0.25 g of catalyst [25]. After the reaction, the solution was filtrated, neutralized by H_2SO_4, and diluted with deionized water. An Agilent 1100 high performance liquid chromatography system equipped with a refractive index detector was applied for product analysis. In addition, an Alltech OA-1000 column was used at a separation temperature of 80 °C. The mobile phase was a H_2SO_4 aqueous solution (0.005 mol/L) operated at a flowrate of 0.5 mL/min. All products were identified using the retention time of pure materials and quantified by an external standard method. The glycerol conversion and liquid product selectivity calculations were conducted using the following equations, with Con. representing the conversion of glycerol, S_a representing the selectivity of product a, R_0 and R_t representing the concentration of glycerol at the reaction time of 0 and *t*, and P_a representing the carbon molar concentration of product *a* at the reaction time of *t*. From our experiment observations and literature reports [15,18,24], the possible gas product was CO_2, which was in trace amount and would be converted to carbonate in any basic solutions present.

$$\text{Con.} = (R_0 - R_t) \times 100\%/R_0$$

$$S_a = P_a \times 100\%/\sum P_a$$

3. Results and discussion

3.1. Characterization of catalysts

3.1.1. N_2 physical adsorption results

Table 1
Textural properties of activated carbon (AC), 5Pt/AC-DP and Pb promoted 5Pt/AC catalysts.

Entry	Catalyst	S_{BET} [a] (m^2/g)	V_{pore} [b] (mL/g)	D_{meso} [c] (nm)	D_{micro} [d] (nm)
1	AC [e]	1241	1.0	4.8	0.4
2	5Pt/AC-DP	1165	1.0	3.8	0.4
3	1Pb-5Pt/AC-Im-DP	1108	0.9	3.8	0.4
4	3Pb-5Pt /AC-Im-DP	1032	0.8	3.0	0.4
5	5Pb-5Pt /AC-Im-DP	889	0.7	3.2	0.4
6	7Pb-5Pt /AC-Im-DP	843	0.6	3.6	0.4
7	5Pb-5Pt /AC-Im-DP-500Ar	898	0.7	4.8	0.4
8	5Pb-5Pt /AC-Co-DP	849	0.6	3.1	0.4
9	5Pb-5Pt /AC-Co-DP-500Ar	917	0.7	4.8	0.4
10	5Pb-5Pt /AC-Co-Im-500H_2	905	0.7	4.0	0.4
11	5Pb-5Pt /AC-Co-Im-500Ar	1039	0.8	4.8	0.4

[a] Calculated by the Brunauer-Emmett-Teller (BET) method.
[b] Determined from the adsorbed nitrogen at a relative pressure (p/p_0) of 0.99.
[c] Calculated on the adsorption curve by the Barrett-Joyner-Halenda (BJH) method.
[d] Derived from the Horvath-Kawazoe (HK) method [27].
[e] Reproduced data from previous work [26].

The N_2 physical adsorption results of the AC support and different catalysts are shown in Table 1 and Fig. 1. The specific surface areas, pore volumes, and average mesopore sizes of 5Pt/AC-DP and *x*Pb-5Pt/AC-Im-DP catalysts were considerably smaller than those of the AC support, whereas the micropore size remained unchanged. This result may be attributed to the partial blockage of mesopores by the deposited metal species [26]. When the Pb loading was increased to more than 3.0 wt%, the catalyst surface areas and pore volumes decreased dramatically, indicating that the blockage was considerable. The blockage was alleviated by treating the samples at 500 °C Ar (or H_2), as shown by the improved surface areas and pore volumes. This result is also shown from the isotherms in Fig. 1, where the introduction of Pb would result in the drop of isotherms, and the 500 °C gas treatment lead to the elevation of isotherms.

3.1.2. XRD analysis

Table 2
Particle sizes of 5Pb-5Pt/AC catalysts calculated from XRD data and the Scherrer equation.

Entry	Catalyst	Pt (nm)	$Pb_3(CO_3)_2(OH)_2$ (nm)	PtPb (nm)	Pt_xPb (nm)
1	5Pb-5Pt /AC-Im-DP	8.8	56.4	–	–
2	5Pb-5Pt /AC-Im-DP-500Ar	13.5	–	47.1	26.0
3	5Pb-5Pt /AC-Co-DP	7.5	60.7	–	–
4	5Pb-5Pt /AC-Co-DP-500Ar	14.9	–	52.5	14.2
5	5Pb-5Pt /AC-Co-Im-500H_2	–	–	–	–
6	5Pb-5Pt /AC-Co-Im-500Ar	13.3	–	–	–

The XRD patterns of the *x*Pb-5Pt/AC-Im-DP catalysts are shown in Fig. 2(a). Characteristic diffraction peaks at 39.8°, 46.2°, 67.5°, and 81.3° are assigned to the Pt(111), (200), (220), and (311) reflections, respectively (JCPDS, 00-004-0802). Metallic Pt particles were present in all the samples. When Pb was supported on the catalysts at a loading of 3.0 wt% or higher, the characteristic reflection peaks of $Pb_3(CO_3)_2(OH)_2$ (JCPDS, 00-013-131) were observed. The major peaks at 34.2°, 27.1°, 24.6°, and 20.9° are indexed as (110), (015), (104), and (012) planes, respectively.

The XRD patterns of 5Pb-5Pt/AC catalysts prepared by different methods are shown in Fig. 2(b). They were denoted with their preparation method because of their same metal loadings. Characteristic Pt peaks were observed in all the 5Pb-5Pt/AC catalysts except Co-Im-500H_2 (sample (5)). This indicates that Pt particles were highly dispersed on the Co-Im-500H_2 catalyst. In contrast, the Co-Im-500Ar (sample (6)) catalyst shows more intense metallic Pt peaks. This result may be related with the availability of reducers during the reduction process, because H_2 (the reducer of Co-Im-500H_2) is more accessible than AC (the reducer of Co-Im-500Ar). From the XRD patterns, the particle sizes of Pt were calculated using the Scherrer equation (Table 2). The 500 °C Ar treatment of Im-DP and Co-DP catalysts also creates larger Pt particles (untreated at 8 nm vs treated at 14 nm).

Similar to the Im-DP catalyst, characteristic peaks of $Pb_3(CO_3)_2(OH)_2$ were also observed in Co-DP catalyst. After 500 °C Ar treatment, these signals disappeared because of the decomposition of $Pb_3(CO_3)_2(OH)_2$ [28]. Platinum lead alloys

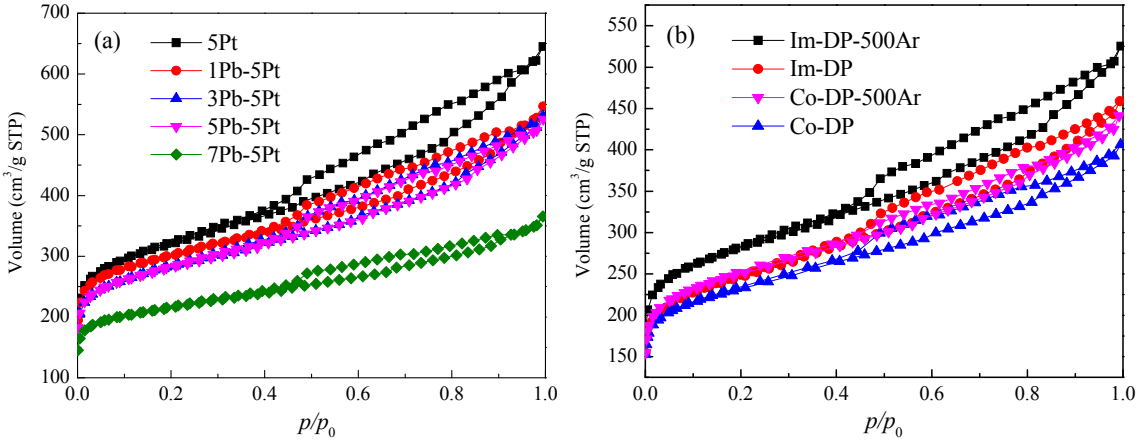

Fig. 1. N_2 physical adsorption-desorption isotherms of *x*Pb-5Pt/AC-Im-DP catalysts (a) and 5Pb-5Pt/AC catalysts prepared by different methods (b).

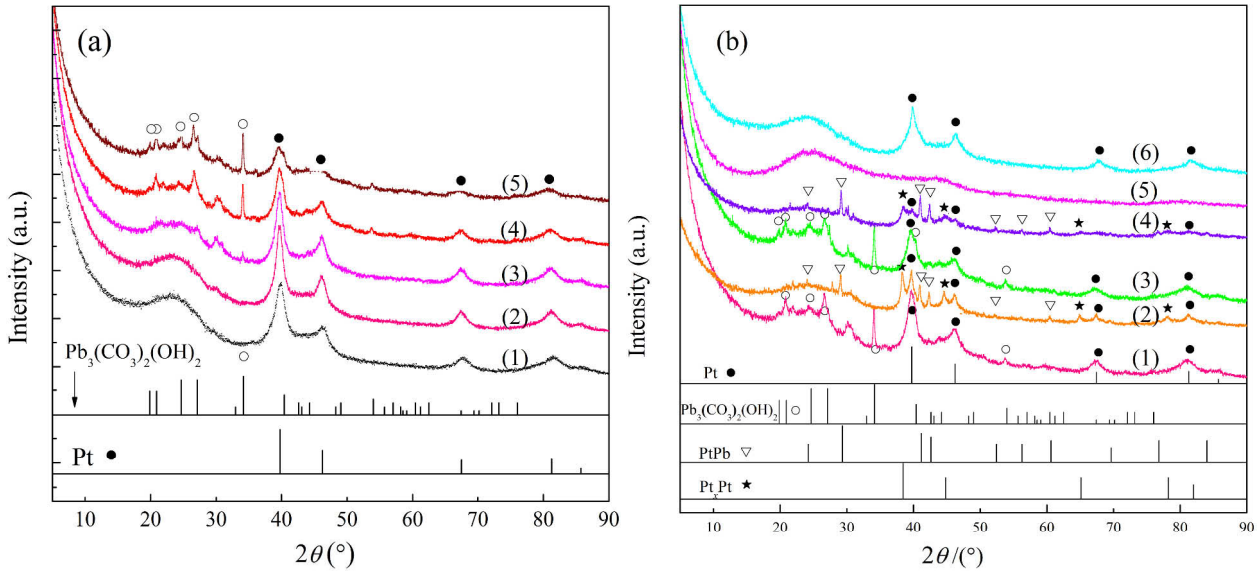

Fig. 2. XRD patterns of different samples. (a): (1) 5Pt/AC-DP, (2) 1Pb-5Pt/AC-Im-DP, (3) 3Pb-5Pt/AC-Im-DP, (4) 5Pb-5Pt/AC-Im-DP, (5) 7Pb-5Pt/AC-Im-DP catalysts; (b): (1) 5Pb-5Pt/AC-Im-DP, (2) 5Pb-5Pt/AC-Im-DP-500Ar, (3) 5Pb-5Pt/AC-Co-DP, (4) 5Pb-5Pt/AC-Co-DP-500Ar, (5) 5Pb-5Pt/AC-Co-Im-500H_2, (6) 5Pb-5Pt/AC-Co-Im-500Ar catalysts. Standard stick patterns of Pt, $Pb_3(CO_3)_2(OH)_2$, PtPb, and Pt_xPb are shown as references.

emerged, i.e., PtPb and Pt_xPb (JCPDS, 00-006-0374 and 00-006-0574). For Co-Im-500H_2 and Co-Im-500Ar catalysts, neither $Pb_3(CO_3)_2(OH)_2$ nor platinum lead alloys were detected.

3.1.3. XPS analysis

The XPS spectra of the *x*Pb-5Pt/AC-Im-DP catalysts were conducted (Fig. 3) to study the oxidation states of the surface metals on the catalysts. The spectra data was processed by a software called XPS Peak 4.1. The backgrounds of curves were subtracted by the Shirley method. A Lorentzian function was convoluted with an experimental Gaussian curve (G = 0.2) for data analysis. The position gap between deconvoluted Pt $4f_{7/2}$ and Pt $4f_{5/2}$ peaks was fixed at 3.3 eV, whereas that for Pb $4f$ peaks was fixed at 5.0 eV. The full width at half maximum of the curve of each group of deconvoluted Pt $4f_{7/2}$ and Pt $4f_{5/2}$ peaks was kept the same, with the peak area of Pt $4f_{5/2}$ being 0.75 times of the area of Pt $4f_{7/2}$. A similar method was applied for the Pb $4f$ spectra.

The Pt $4f$ spectra of monometallic 5Pt/AC-DP catalyst and bimetallic *x*Pb-5Pt/AC-Im-DP catalysts are shown in Fig. 3(a),

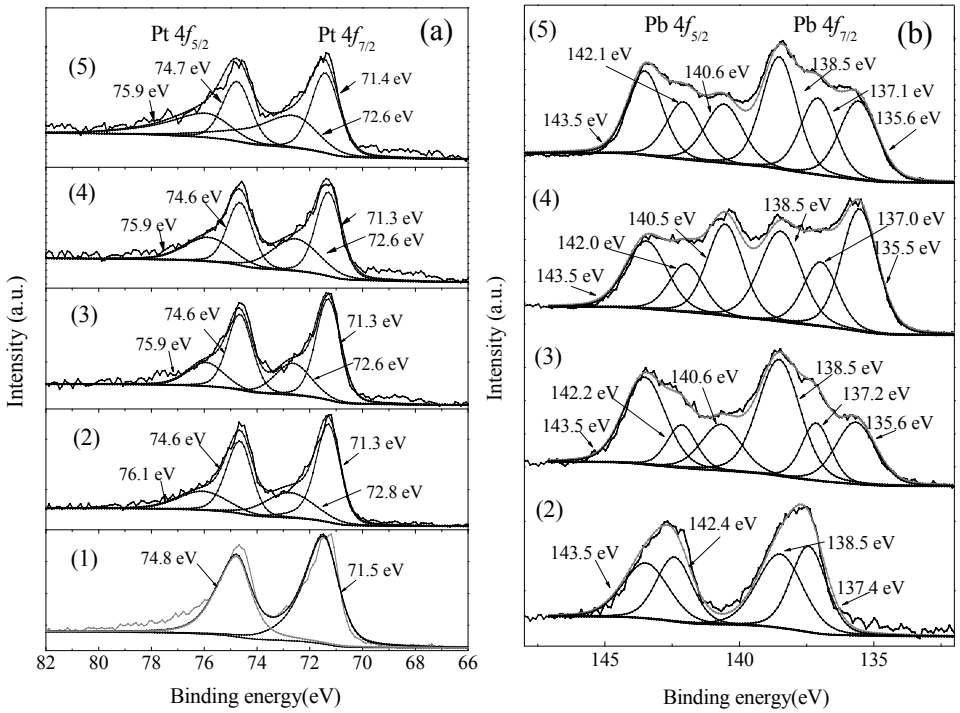

Fig. 3. XPS spectra of Pt $4f$ (a) and Pb $4f$ (b). (1) 5Pt/AC-DP, (2) 1Pb-5Pt/AC-Im-DP, (3) 3Pb-5Pt/AC-Im-DP, (4) 5Pb-5Pt/AC-Im-DP, (5) 7Pb-5Pt/AC-Im-DP catalysts.

with two doublet peaks originated from the spin-orbital splitting of the Pt $4f_{7/2}$ and Pt $4f_{5/2}$ states. The deconvoluted peaks of monometallic 5Pt/AC-DP catalyst at 71.5 and 74.8 eV were ascribed to the metallic form of Pt, meaning that its surface Pt species generally remained unoxidized [26]. However, for Pb-promoted catalysts, the deconvoluted peaks at 72.6–72.8 and 75.9–76.1 eV indicate the presence of oxidized Pt species, similar to the results in our previous report [16].

For Pb 4*f* spectra in Fig. 3(b), the binding energy (BE) peaks were deconvoluted into two or three groups. The BE peaks at 138.5, 137.0–137.4, and 135.5–135.6 eV were ascribed to the Pb^{4+}, Pb^{2+}, and Pb^0 species, respectively [29–31]. Unlike samples (3), (4), and (5), almost no Pb^0 species was detected on the surface of the 1Pb-5Pt/AC-Im-DP catalyst. Therefore, the overall oxidation state of Pb species on 1Pb-5Pt/AC-Im-DP is higher than other *x*Pb-5Pt/AC-Im-DP catalysts, influencing the oxidation state of the surface Pt species, which showed a higher BE peak at 72.8 eV than the other three catalysts at 72.6 eV (Fig. 3(a)).

To observe the influence of the 500 °C Ar treatment on the metal oxidation state, two representative 5Pb-5Pt/AC catalysts (i.e., the Co-DP and the Co-DP-500Ar catalysts) were adopted for XPS analysis (Fig. 4). The Pt 4*f* peaks (slightly) and the Pb 4*f* peaks (obviously) shifted to a lower BE position after Ar treatment at 500 °C. Considering that carbon is frequently used as a reducing agent, the treatment of Co-DP catalyst may favor the reduction of metals by the AC support. In addition, the Pt 4*f* peaks of 5Pb-5Pt/AC-Co-DP (Fig. 4(a), sample (1)) and 5Pb-5Pt/AC-Im-DP catalysts (Fig. 3(a), sample (4)) were of similar shape and position, whereas their Pb 4*f* peaks were obviously different (Fig. 4(b) vs Fig. 3(b)). In a previous discussion, these two catalysts were of similar XRD patterns (Fig. 2(b)), but the XPS analysis demonstrated that their surface Pb species were different, which would result in different catalytic performance.

3.1.3. TEM analysis

The TEM images of two groups of representative catalysts (Im-DP vs Im-DP-500Ar, Co-DP vs Co-DP-500Ar) are presented in Fig. 5. The Ar treatment at 500 °C resulted in the metal particle aggregation (Fig. 5(b) vs Fig. 5(d)), which agrees with the XRD results. The HR-TEM images demonstrated the respective characteristic lattice fringes of the metallic particles. In images of Im-DP and Co-DP, only characteristic patterns of Pt (111) planes (d = 2.28 Å) (JCPDS, 00-004-0802) were observed. However, PtPb alloys (JCPDS, 00-006-0374) were also detected in Im-DP-500Ar and Co-DP-500Ar images. In Im-DP-500Ar, PtPb(101) planes (d = 3.04 Å) were observed, whereas in Co-DP-500Ar, PtPb (100) and (102) planes with d = 3.68 and d = 2.20 Å, respectively, were observed. This also agrees with the XRD analysis that Ar thermal treatment favored the Pt-Pb alloys formation.

3.2. Selective oxidation of glycerol

3.2.1. Optimization of Pb loading for xPb-5Pt/AC-Im-DP catalysts

Table 3 shows the results of glycerol oxidation reactions over 5Pt/AC-DP and *x*Pb-5Pt/AC-Im-DP catalysts with Pb loading ranging from 1.0 to 7.0 wt%. From our previous optimization studies of alkaline salts and their ratios, we adopted LiOH in this work [25]. Although the monometallic Pb/AC cat-

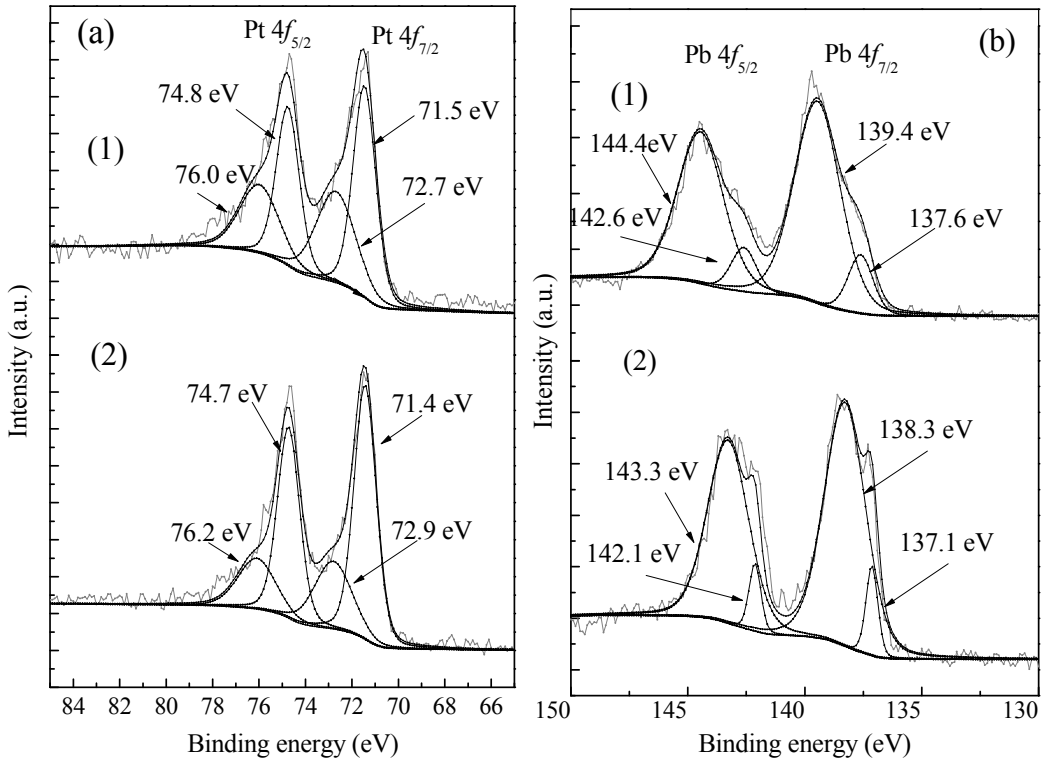

Fig. 4. XPS spectra of Pt 4*f* (a) and Pb 4*f* (b). Samples: (1) 5Pb-5Pt/AC-Co-DP, (2) 5Pb-5Pt/AC-Co-DP-500Ar.

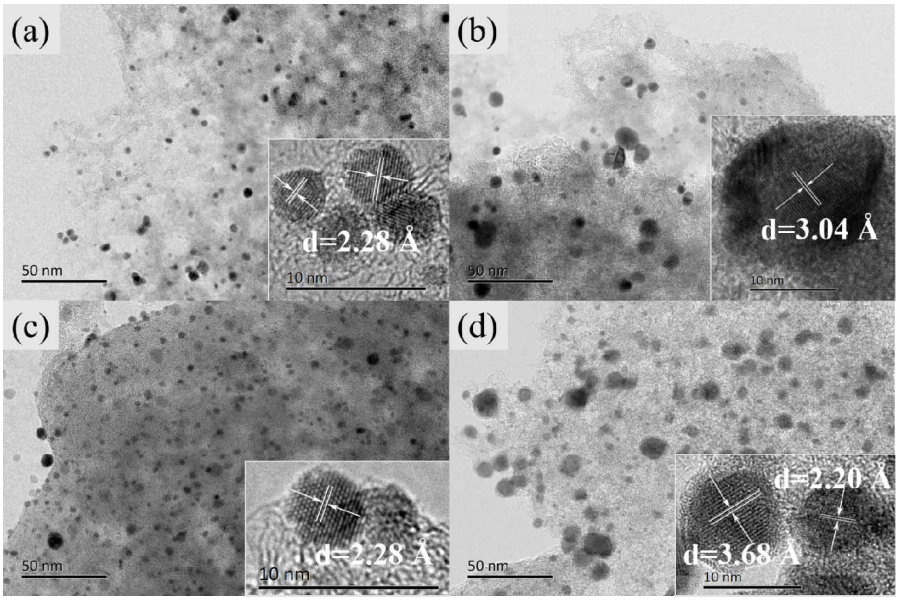

Fig. 5. TEM images of Im-DP (a); Im-DP-500Ar (b); Co-DP (c); and Co-DP-500Ar (d) catalysts. The insets are high resolution images showing their characteristic lattice fringes.

alyst showed no activity in converting glycerol (data not shown), the addition of 1.0 wt% Pb to 5Pt/AC catalyst improved catalyst turnover frequency (TOF) compared with the monometallic 5Pt/AC-DP catalyst. For other *x*Pb-5Pt/AC-Im-DP catalysts, the increase of Pb loading resulted in a decrease in catalyst TOF (as well as glycerol conversion), and the changing trend is consistent with that of their N_2 physical adsorption data. This result indicates that the decrease in surface area and pore size can cause the decrease in catalyst activity (Table 1).

As shown in the XRD analysis (Fig. 2(a)), the increase in Pb loading (> 1.0 wt%) leads to $Pb_3(CO_3)_2(OH)_2$ formation. This might be one of the reasons for the decreased surface area and pore volume. For the 1Pb-5Pt/AC-Im-DP catalyst, although its surface area was smaller, its catalytic performance is higher than that of 5Pt/AC-DP, and no characteristic peaks for $Pb_3(CO_3)_2(OH)_2$ were detected. Therefore, $Pb_3(CO_3)_2(OH)_2$ might be the main reason for the catalyst activity decrease at high Pb loading (> 1.0 wt%).

In addition, the analysis of Pb 4*f* spectra (Fig. 3(b)) of *x*Pb-5Pt/AC-Im-DP catalysts suggested that surface Pb^0 species are unfavorable for the glycerol conversion. Because the Pb^0 species were observed in all *x*Pb-5Pt/AC-Im-DP catalysts except the 1Pb-5Pt/AC-Im-DP catalyst. The role of Pt species in the enhanced glycerol conversion of the 1Pb-5Pt/AC-Im-DP catalyst could not be determined, because Pt^0 and Pt^{2+} species were detected in all the bimetallic catalysts (Fig. 3(a)).

Table 3
Effects of Pb loading on glycerol conversion and product selectivity for *x*Pb-5Pt/AC-Im-DP catalysts [a].

Catalyst	TOF (h^{-1}) [b]	Time (h)	Conversion (%)	Selectivity (%)							
				PA [c]	LA	GLYA	TA	GA	OA	AA	FA
5Pt/AC-DP	76.7	2	36.2	0.9	68.3	15.5	2.6	7.8	1.6	1.9	1.4
		6	96.3	0.6	67.7	11.9	5.5	5.7	1.6	2.8	4.2
		10	100	2.8	44.9	1.5	21.9	2.2	22.0	4.6	0.1
1Pb-5Pt/AC-Im-DP	100.8	2	47.6	1.7	61.8	15.3	3.4	9.8	3.6	2.2	2.1
		6	92.3	1.6	56.5	14.9	7.9	6.5	4.5	7.5	0.7
		10	100	8.7	36.7	7.7	17.9	2.7	12.5	13.0	0.7
3Pb-5Pt /AC-Im-DP	74.5	2	35.2	1.2	55.1	21.1	5.1	7.8	5.1	2.4	2.1
		6	80.7	1.5	53.6	20.1	9.3	5.4	5.5	4.0	0.6
		10	98.9	8.6	34.3	12.9	22.3	3.2	12.6	9.3	0.4
5Pb-5Pt /AC-Im-DP	70.3	2	33.2	0.8	61.8	19.0	3.9	6.6	4.0	2.0	1.8
		6	80.4	1.4	63.3	17.7	5.9	3.8	3.0	4.3	0.6
		10	100	14.2	34.9	9.8	19.5	2.0	9.1	10.2	0.3
7Pb-5Pt /AC-Im-DP	72.6	2	34.3	0.8	61.5	21.3	5.1	4.2	3.7	2.2	1.3
		6	88.3	1.3	61.2	19.1	7.0	3.4	3.9	3.7	0.4
		10	100	9.7	35.4	12.6	19.8	2.8	9.4	9.9	0.5

[a] Reaction conditions: t = 90 ℃, p = 1 atm, F_{O_2} = 100 mL/min, $n_{LiOH}/n_{glycerol}$ = 1.5, stirring rate = 800 r/min. [b] TOF was calculated based on the loading of Pt since Pb mainly served as a promoter, and the 2 h reaction data was used for the calculation. [c] PA = pyruvic acid, LA = lactic acid, GLYA = glyceric acid, TA = tartronic acid, GA = glycolic acid, OA = oxalic acid, AA = acetic acid, FA = formic acid.

In terms of the target product PA, the introduction of Pb showed enhanced PA selectivity, which may be because of the presence of Pb and the generation of oxidized Pt species in all the four *x*Pb-1Pt/AC-Im-DP catalysts, which was caused by the Pb promoter as shown in the XPS analysis (Fig. 3(a)). From the product distributions, the introduction of Pb favored PA production and contributed to glyceric acid selectivity. However, the productions of LA and oxalic acid were decreased. This result may be because the presence of Pb favored LA consecutive oxidation towards PA, but not glyceric acid consecutive oxidation and C–C cleavage reaction to oxalic acid [32]. The 5Pb-5Pt/AC-Im-DP catalyst showed the highest performance with a PA selectivity over 14%.

3.2.2. *Further investigation on the roles of Pt and Pb species*

To further explore the previous speculation on the roles of surface Pb^0 species and $Pb_3(CO_3)_2(OH)_2$, we prepared a series of 5Pb-5Pt/AC catalysts by different methods. Fig. 6(a) shows the catalyst TOF, and Fig. 6(b) shows the glycerol conversion over these 5Pb-5Pt/AC catalysts with time on stream. As discussed in Section 3.2.1, the decreases in glycerol conversion were related with the Pb^0 species. The comparison of catalyst TOF in Fig. 6(a) and glycerol conversion in Fig. 6(b) between Im-DP and Co-DP could further investigate the role of Pb^0 species. The XRD patterns of Im-DP and Co-DP were similar (Fig. 2), with $Pb_3(CO_3)_2(OH)_2$ observed in both of them. Their Pt 4f spectra were also of similar shape and position. However, their Pb 4f spectra (Fig. 3(b) sample (4) vs Fig. 4(b) sample (1)) were different, with the Pb^0 species present only in the Im-DP catalyst. Thus, the lower TOF and glycerol conversion of the Im-DP catalyst might be related with the Pb^0 species.

The role of $Pb_3(CO_3)_2(OH)_2$ could be illustrated by the following comparison. For the Im-DP and Co-DP catalysts, their TOF and glycerol conversions were generally enhanced after treatment under Ar at 500 °C. On the one hand, this suggests that the removal of $Pb_3(CO_3)_2(OH)_2$ might be beneficial to glycerol conversion. On the other hand, such an improvement might be related with the formation of PtPb and Pt_xPb alloys. The BE peak shift of Pb to a lower state might be associated with the catalyst performance. The decomposition of

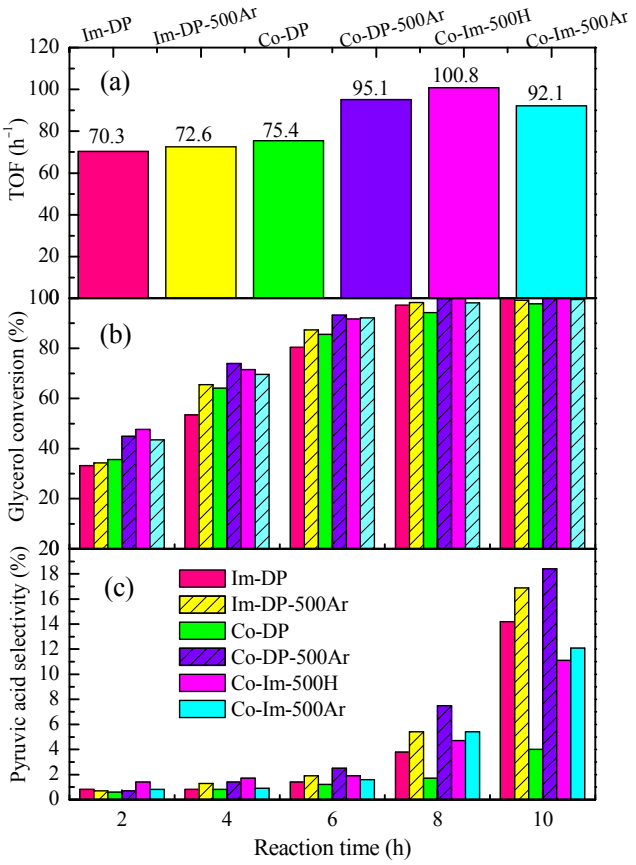

Fig. 6. Effects of preparation method of 5Pb-5Pt/AC catalysts on: catalyst TOF (a); Glycerol conversion (b); and PA selectivity (c). Reaction conditions: t = 90 °C, p = 1 atm, F_{O_2} = 100 mL/min, $n_{LiOH}/n_{glycerol}$ = 1.5, stirring rate = 800 r/min.

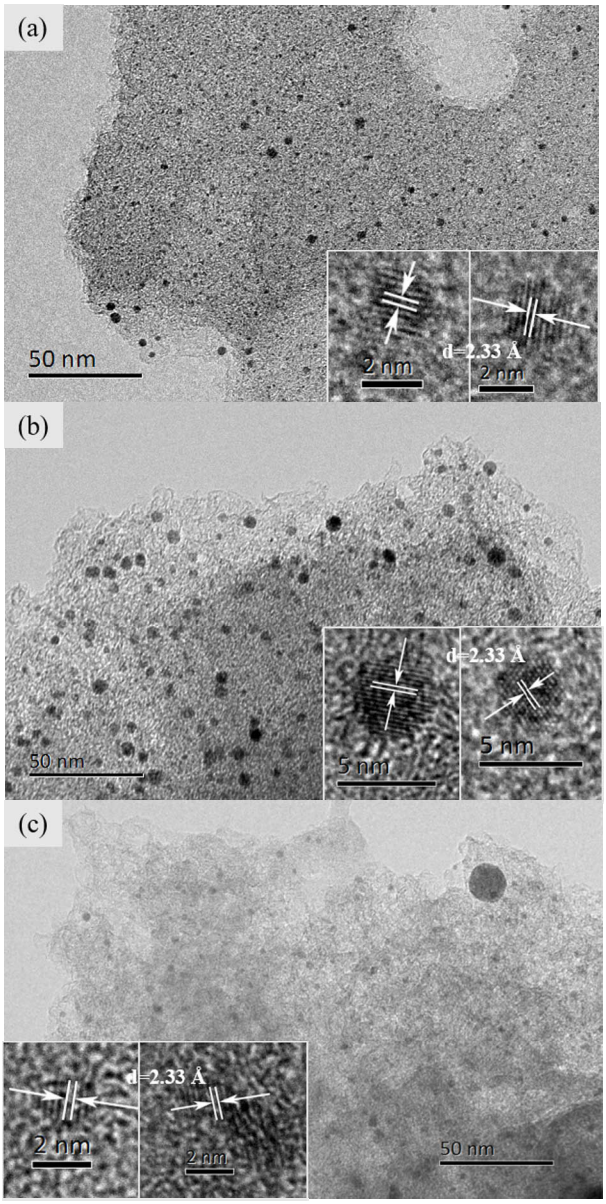

Fig. 7. TEM images of spent Co-DP (a); Co-DP-500Ar (b) and Co-Im-500Ar (c) catalysts. The insets are high resolution images showing their characteristic lattice fringes. A d = 2.33 Å from the patterns is characteristic of Pt_xPb (111) planes (JCPDS, 00-006-0574).

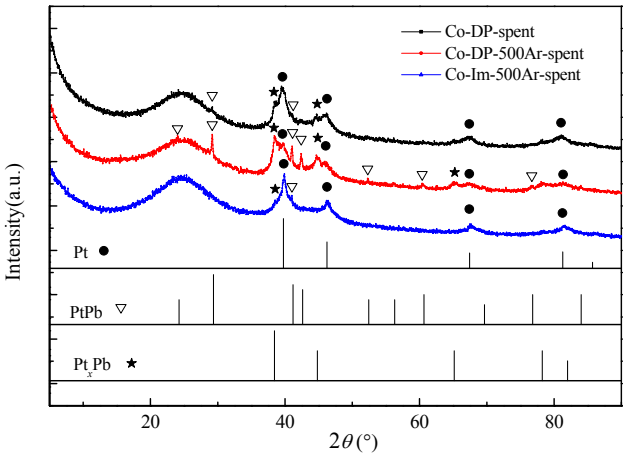

Fig. 8. XRD patterns of spent Co-DP, Co-DP-500Ar and Co-Im-500Ar catalysts. Stick patterns of Pt, PtPb, and Pt_xPb are shown as references.

$Pb_3(CO_3)_2(OH)_2$ and the formation of Pt_xPb alloys can cause a BE peak shift. Thus, further analysis is still necessary to clarify the mechanism. For simplicity, the following discussion focuses on the $Pb_3(CO_3)_2(OH)_2$ and Pt_xPb alloy species. For Co-Im-500H_2 and Co-Im-500Ar catalysts, Ar or H_2 treatment at 500 °C prevented $Pb_3(CO_3)_2(OH)_2$ formation; moreover, neither PtPb nor Pt_xPb alloys were observed. They still showed higher TOF and glycerol conversion than the Im-DP and Co-DP catalysts. Therefore, the removal of $Pb_3(CO_3)_2(OH)_2$ is essential for enhancing catalyst activity.

Similar to the enhancement effect on catalyst activity, the PA selectivities of Im-DP and Co-DP catalysts were improved after their treatment at 500 °C in Ar (Fig. 6(c)). The PA selectivity of Co-DP-500Ar was almost 4.6 times higher than that of the untreated Co-DP catalyst, the PA yield reached 18.4% under the present reaction conditions. Thus, the PA selectivity might also be related with the removal of $Pb_3(CO_3)_2(OH)_2$ and the formation of platinum lead alloys.

The role of PtPb and Pt_xPb alloys could be partly demonstrated by the comparison between the Co-DP-500Ar and the Co-Im-500Ar catalysts. In both cases, the Pt and Pb metals were reduced simultaneously on AC, and their calculated Pt particle sizes were similar (Table 2). The Co-DP-500Ar catalyst contains two more species than the Co-Im-500Ar catalyst, which were the PtPb and Pt_xPb alloys. The former catalyst showed slightly better glycerol conversion and much improved PA selectivity than those of the latter one (Fig. 6). Therefore, the platinum lead alloys might favor the glycerol activation slightly and its transformation towards PA greatly. For fresh catalysts with PtPb and Pt_xPb alloys present (i.e., Im-DP-500Ar and Co-DP-500Ar catalysts), their PA selectivity maintained the highest among all the catalysts tested.

We characterized three representative spent catalysts (i.e., Co-DP, Co-DP-500Ar and Co-Im-500Ar catalysts, with three different phases), to find more information about the role of platinum lead alloys. The alloys were observed only on fresh Co-DP-500Ar catalyst, yet they were observed on all the three spent catalysts, as confirmed by both HR-TEM and XRD analyses (Figs. 7 and 8). In addition, the XPS analysis of spent Co-DP and Co-DP-500Ar showed that the Pb 4*f* peak of Co-DP shifted

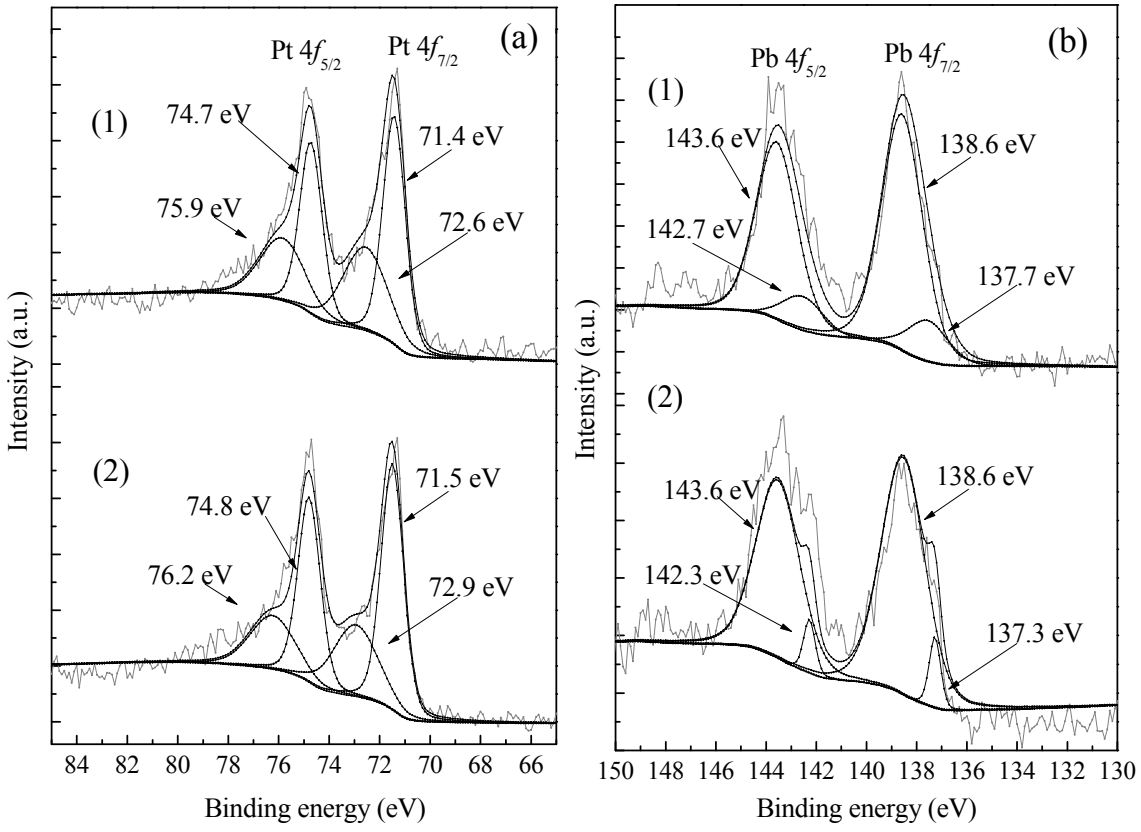

Fig. 9. Pt 4*f* (a) and (b) Pb 4*f* XPS spectra of spent 5Pb-5Pt/AC-Co-DP (1) and spent 5Pb-5Pt/AC-Co-DP-500Ar (2).

Table 4
Glycerol conversion and product selectivity over spent 5Pb-5Pt/AC catalysts[a].

Catalyst	Conversion (%)	Selectivity (%)							
		PA[b]	LA	GLYA	TA	GA	OA	AA	FA
5Pb-5Pt /AC-Co-DP-Spent	100	6.1	47.4	15.2	13.8	2.2	6.5	7.3	1.5
5Pb-5Pt/AC-Co-Im-500Ar-Spent	97.0	12.2	37.5	15.7	17.1	15.7	5.6	9.4	0.0

[a] Reaction conditions: t = 90 ℃, p = 1 atm, 10 h, F_{O_2} = 100 mL/min, $n_{LiOH}/n_{glycerol}$ = 1.5, stirring rate = 800 r/min.
[b] See Table 3.

from 139.4 to 138.6 eV (Fig. 4(b) vs Fig. 9(b)) after the reaction. The surface Pb species on Co-DP-500Ar catalyst remain the same before and after the reaction, whereas the Pb species on spent Co-DP catalysts resemble that of the spent Co-DP-500Ar catalyst, which agrees with the HR-TEM and XRD results. The spent Co-DP and Co-DP-500Ar catalysts were evaluated under the same reaction conditions, and they exhibited slightly better PA selectivity than the fresh ones (Table 4). This suggested that the PtPb and Pt_xPb alloys might be the active sites for PA production. However, their formation and catalytic mechanisms still require further investigation.

We propose a possible reaction pathway for glycerol oxidation to PA and other products (Scheme 1). Glycerol is first dehydrogenated to form intermediates, followed by their dehydration and intramolecular Cannizzaro rearrangement to LA [33,21]. The introduction of Pb was beneficial for glycerol conversion when $Pb_3(CO_3)_2(OH)_2$ and surface Pb^0 species were absent, and the presence of platinum lead alloys favored the transformation of LA to PA.

4. Conclusions

A one-step production of PA by selective oxidation of glycerol was investigated. Both the Pb loading and the preparation methods greatly affect the catalyst performance, because of the alteration of Pt and Pb species. The Pt-Pb alloys are favorable for glycerol transformation to PA, whereas the $Pb_3(CO_3)_2(OH)_2$ and the surface Pb^0 species adversely affect glycerol conversion. By treating the 5Pb-5Pt/AC-Im-DP (or 5Pb-5Pt/AC-Co-DP) catalyst under a 500 °C Ar atmosphere, $Pb_3(CO_3)_2(OH)_2$ can be prevented, and platinum lead alloys can form. The highest PA yield was 18.4% under the present reaction conditions. Further optimization and better understanding of the reaction are required.

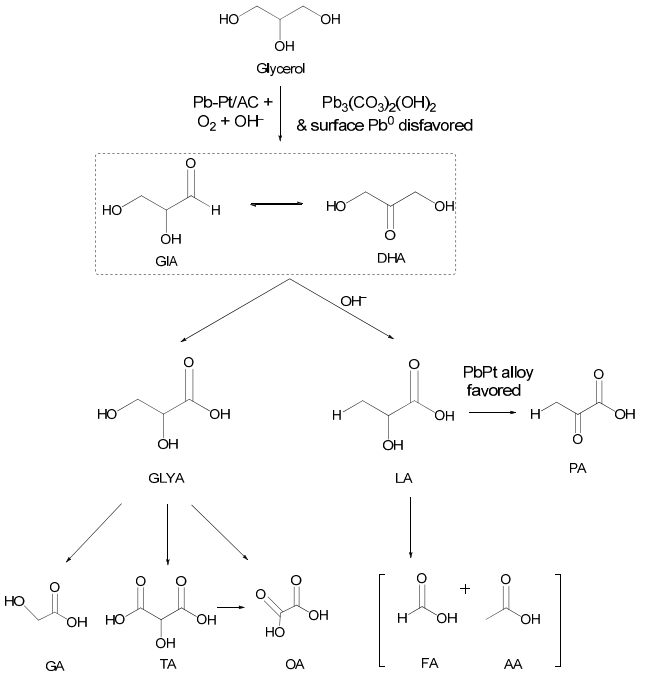

Scheme 1. Proposed mechanism for selective oxidation of glycerol over xPb-5Pt/AC catalysts.

References

[1] S. Bagheri, N. M. Julkapli, W. A. Yehye. *Renewable Sustainable Energy Rev.*, **2015**, 41, 113–127.
[2] M. Anitha, S. K. Kamarudin, N. Kofli. *Chem. Eng. J.*, **2016**, 295, 119–130.
[3] C. H. Zhou, J. N. Beltramini, Y. X. Fan, G. Q. Lu. *Chem. Soc. Rev.*, **2008**, 37, 527–549.
[4] B. Katryniok, H. Kimura, E. Skrzyńska, J. S. Girardon, P. Fongarland, M. Capron, R. Ducoulombier, N. Mimura, S. Paul, F. Dumeignil. *Green Chem.*, **2011**, 13, 1960–1979.
[5] A. Villa, N. Dimitratos, C. E. Chan-Thaw, C. Hammond, L. Prati, G. J. Hutchings. *Acc. Chem. Res.*, **2015**, 48, 1403–1412.
[6] L. F. Gong, Y. Lu, Y. J. Ding, R. H. Lin, J. W. Li, W. D. Dong, T. Wang, W. M. Chen. *Appl. Catal. A*, **2010**, 390, 119–126.
[7] W. T. Luo, Y. Lyu, L. F. Gong, H. Du, M. Jiang, Y. J. Ding. *Chin. J. Catal.*, **2016**, 37, 2009–2017.
[8] G. S. Foo, D. Wei, D. S. Sholl, C. Sievers. *ACS Catal.*, **2014**, 4, 3180–3192.
[9] C. J. Jia, Y. Liu, W. Schmidt, A. H. Lu, F. Schüth. *J. Catal.*, **2010**, 269, 71–79.
[10] M. Dusselier, P. Van Wouwe, A. Dewaele, E. Makshina, B. F. Sels. *Energy Environ. Sci.*, **2013**, 6, 1415–1442.
[11] A. Corma, S. Iborra, A. Velty. *Chem. Rev.*, **2007**, 107, 2411–2502.
[12] P. Xu, J. H. Qiu, C. Gao, C. Q. Ma. *J. Biosci. Bioeng.*, **2008**, 105, 169–175.
[13] T. Yasukawa, W. Ninomiya, K. Ooyachi, N. Aoki, K. Mae. *Ind. Eng. Chem. Res.*, **2011**, 50, 3858–3863.
[14] H. H. C. M. Pinxt, B. F. M. Kuster, G. B. Marin. *Appl. Catal. A.*, **2000**, 191, 45–54.
[15] T. Tsujino, S. Ohigashi, S. Sugiyama, K. Kawashiro, H. Hayashi. *J. Mol. Catal.*, **1992**, 71, 25–35.
[16] C. Zhang, T. Wang, Y. J. Ding. *Appl. Catal. A*, **2017**, 533, 59–65.
[17] T. V. Finogenova, I. G. Morgunov, S. V. Kamzolova, O. G. Chernyavskaya. *Appl. Biochem. Microbiol.*, **2005**, 41, 418–425.
[18] S. Sugiyama, T. Kikumoto, H. Tanaka, K. Nakagawa, K. I. Sotowa, K. Maehara, Y. Himeno, W. Ninomiya. *Catal. Lett.*, **2009**, 131, 129–134.
[19] M. Ai. *Appl. Catal. A*, **2002**, 234, 235–243.
[20] L. S. Sharninghausen, J. Campos, M. G. Manas, R. H. Crabtree. *Nat.*

Graphical Abstract

Chin. J. Catal., 2017, 38: 928–938 doi: 10.1016/S1872-2067(17)62835-3

One-step synthesis of pyruvic acid from glycerol oxidation over Pb promoted Pt/activated carbon catalysts

Chen Zhang, Tao Wang *, Yunjie Ding*
Dalian Institute of Chemical Physics, Chinese Academy of Sciences; University of Chinese Academy of Sciences

Over 18% yield of pyruvic acid was obtained over Pb-Pt/AC catalyst through one-step glycerol oxidation reaction under mild conditions. Both Pb loading and preparation method influenced catalyst activity.

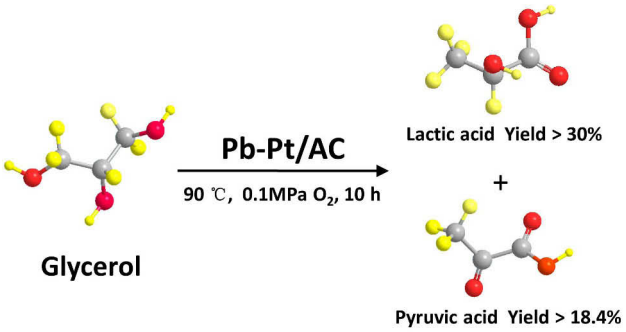

Commun., **2014**, 5, 5084.
[21] Y. H. Shen, S. H. Zhang, H. J. Li, Y. Ren, H. C. Liu. *Chem. Eur. J.*, **2010**, 16, 7368–7371.
[22] R. K. P. Purushothaman, J. van Haveren, D. S. van Es, I. Melián Cabrera, J. D. Meeldijk, H. J. Heeres. *Appl. Catal. B*, **2014**, 147, 92–100.
[23] D. Roy, B. Subramaniam, R. V. Chaudhari. *ACS Catal.*, **2011**, 1, 548–551.
[24] H. Hayashi, S. Sugiyama, Y. Katayama, K. Kawashiro, N. Shigemoto. *J. Mol. Catal.*, **1994**, 91, 129–137.
[25] C. Zhang, T. Wang, X. Liu, Y. J. Ding. *Chin. J. Catal.*, **2016**, 37, 502–509.
[26] C. Zhang, T. Wang, X. Liu, Y. J. Ding. *J. Mol. Catal. A*, **2016**, 424, 91–97.
[27] S. Y. Lee, S. J. Park. *Carbon*, **2014**, 68, 112–117.
[28] S. Sarig, F. Kahana. *Thermochim. Acta*, **1976**, 14, 263–268.
[29] W. E. Morgan, J. R. Van Wazer. *J. Phys. Chem.*, **1973**, 77, 964–969.
[30] V. I. Nefedov, Y. V. Salyn, P. M. Solozhenkin, G. Y. Pulatov. *Surf. Interface Anal.*, **1980**, 2, 170–172.
[31] J. A. Taylor, D. L. Perry. *J. Vac. Sci. Technol. A*, **1984**, 2, 771–774.
[32] E. G. Rodrigues, S. A. C. Carabineiro, J. J. Delgado, X. Chen, M. F. R. Pereira, J. J. M. Órfão. *J. Catal.*, **2012**, 285, 83–91.
[33] S. E. Davis, M. S. Ide, R. J. Davis. *Green Chem.*, **2013**, 15, 17–45.

Page numbers refer to the contents in the print version, which include both the English version and extended Chinese abstract of the paper. The online version only has the English version. The pages with the extended Chinese abstract are only available in the print version.